A THEORY FOR OPTIMAL MTI (MOVING TARGET INDICATOR) DIGITAL SIGNAL PROCESSING: PART II. SIGNAL DESIGN

Robert J. McAulay

Massachusetts Institute of Technology

Prepared for:

Department of the Air Force

4 October 1972

MASSACHUSETTS INSTITUTE OF TECHNOLOGY
LINCOLN LABORATORY

A THEORY FOR OPTIMAL MTI DIGITAL SIGNAL PROCESSING
PART II. SIGNAL DESIGN

R. J. McAULAY

Group 41

TECHNICAL NOTE 1972-14
(Part II)

4 OCTOBER 1972

LEXINGTON MASSACHUSETTS

The work reported in this document was performed at Lincoln Laboratory, a center for research operated by Massachusetts Institute of Technology, with the support of the Department of the Air Force under Contract F19628-73-C-0002.

ABSTRACT

In Part I of this report the optimum MTI receiver was derived and analyzed for the case in which the radar pulses were emitted from the transmitter equally spaced in time. For typical long range ATC surveillance radars, aliasing of the target and clutter spectra results in detection blind speeds at multiples of approximately 70 knots. It is well known operationally that these blind speeds can be eliminated by staggering the transmitter PRF. Heretofore, there has been no thorough theoretical analysis of the effect of staggered PRF on the spectral distribution of the target and clutter signals. It is shown in Part II that the clutter spectral density continues to fold over at the PRF, but that the signal spectrum becomes dispersed in frequency, somewhat like an anti-jam signal. The effect that this phenomenon has on the performance of the optimum processor is evaluated in terms of the signal-to-interference ratio (SIR) criterion that was derived in Part I.

It is further noted that even when the target Doppler shifts are more than one PRF apart, the spectra are distinguishable, suggesting that unambiguous Doppler estimation may be possible. This concept is explored in detail using the MTI ambiguity function. It is shown that good SIR performance can be obtained by choosing the stagger parameters to minimize the height of the subsidiary Doppler side-lobes. The resulting design problem is noted to be similar to that of obtaining good antenna patterns for arrays having non-uniformly spaced elements.

Accepted for the Air Force
Joseph J. Whelan, USAF
Acting Chief, Lincoln Laboratory Liaison Office

A Theory for Optimal MTI Digital Signal Processing

Part II: Signal Design

I. INTRODUCTION AND SYNOPSIS

In Part I of this report [1] statistical decision theoretical methods were used to develop a rational basis for comparing the performance of MTI receivers. The analysis has led to the development of a new receiver structure that is practical to implement using digital signal processing (DSP) techniques and achieves essentially optimum performance. All of the results in Part I were based on the assumption that pulses leave the transmitter uniformly spaced in time. For en-route L-band radars in which the unambiguous range must be 200 n. mi., unambiguous velocity measurements are not possible because of target spectrum aliasing at the PRF. Furthermore, the clutter spectrum also folds over at the PRF resulting in "blind speeds" at which the detection SNR of even the optimal detector is degraded below practically useful limits. This effect is demonstrated in Figure 1. In the development of classical MTI processing it has been found from intuitive considerations that if the transmitter pulses are staggered in time, improved detection performance can be obtained [2], [3]. However, there has been no thorough theoretical investigation of the exact effect that staggered PRF's have on the underlying target and clutter models. The analysis developed in Part I is generalized in this report to allow for the non-uniformly spaced sampling pattern. In Section II, models are derived for the sampled-data target and

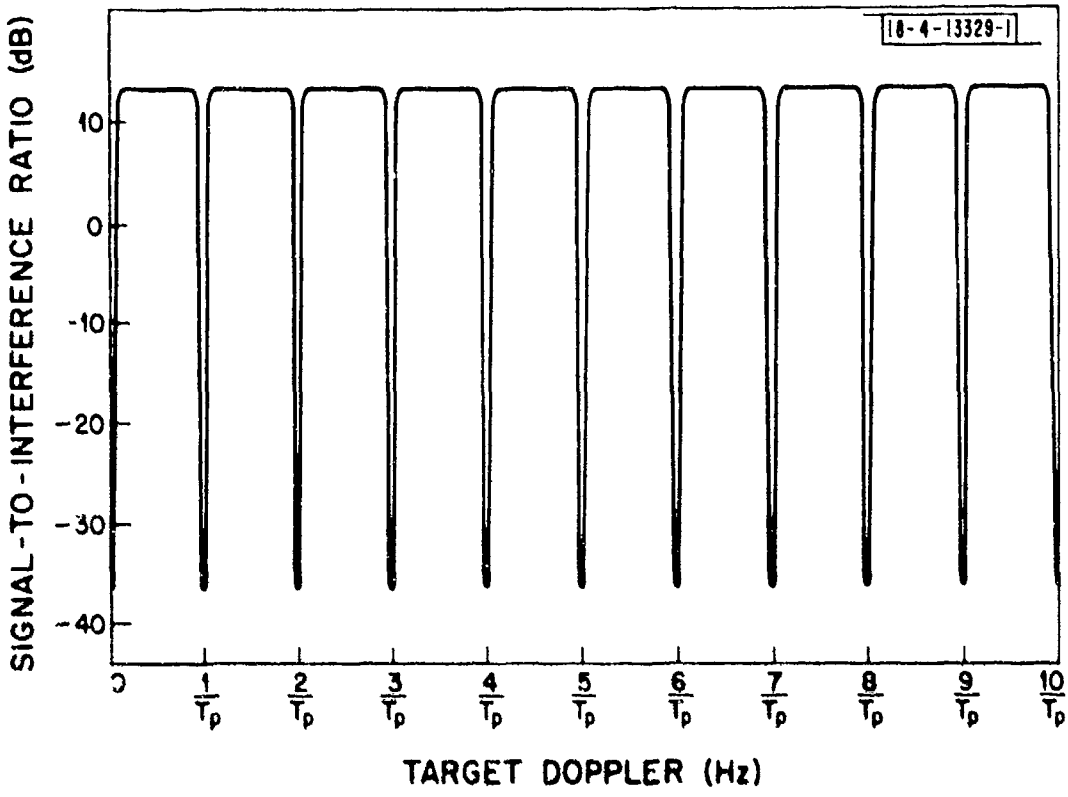

Fig. 1. Optimum ARSR SIR performance using uniform sampling.

clutter returns that result when a range ring is sampled by repetitive bursts of M non-uniformly spaced pulses. The resulting model is used in conjunction with the decision theoretical test of Part I to derive the optimum receiver structure. As in the uniformly sampled case, the processor consists of a clutter rejection filter and a bank of matched filters that are in a sense matched to the target signal over the enlarged unambiguous velocity region. It is shown that this enlarged complex of matched filters can be realized by making appropriate interconnections of filters that extend over only the original ambiguous frequency interval. Hence, it may very well be practical to implement the optimum processor using DSP techniques. The Signal-to-Interference (SIR) performance measure is used to evaluate the performance of the optimum detector and it is shown that reasonable detection can be achieved at velocities that previously could not be seen by the radar. In addition to providing better detection performance over a larger velocity interval, the optimal processor is capable of providing velocity estimates over the larger velocity range. Since staggering the PRF increases the unambiguous velocity interval at the expense of a decrease in the unambiguous range interval, it is clear that the ambiguity surface of the transmitted waveform is being altered. Therefore, staggering the PRF is basically an MTI signal design problem and hence is characterized by the range-velocity ambiguity function. This function is evaluated along the Doppler axis as this represents the output of the matched filters of the optimal processor. It is shown that the M-pulse staggered waveform reduces the velocity ambiguity at the average PRF.

II. INTRODUCTION TO MTI SIGNAL DESIGN

The analysis presented in Part I has led to the development of a quantitative technique for evaluating optimal and suboptimal MTI receivers. The results show that a considerable improvement in target detection capability is possible using the matched filter receiver. The problem formulation and receiver synthesis are based on the assumption that the sampling rate is uniform. In that case, for the L-band ARSR [4], an aircraft moving at 600 kts. induces a Doppler shift corresponding to 3000 Hz. Since the PRF needed to obtain 200 nmi. unambiguous range is 360 pulses/sec., aliasing of the target and clutter spectra will occur with period 360 Hz. or 72 kts. Therefore if an aircraft is moving at a velocity $\pm$ n x 72 kts. n = 0,1,2,..., the Signal-To-Interference-Ratio (SIR) will be seriously degraded due to the clutter aliasing. Furthermore it will be impossible to distinguish between a target moving at velocity v and another at v $\pm$ n x 72. Since staggering the PRF has been found to improve the detection capabilities of MTI receivers at the blind speeds [2] it is of interest to determine the theoretical basis for this improvement and to explore its implications regarding the question of velocity resolution. Since the underlying statistical properties of the data samples will be affected by the non-uniform sampling pattern, it is necessary to re-examine the basic target and clutter models that were derived in Part I for the uniformly sampled system.

Target Model

It was shown in Section II of Part I, that if the aircraft induced a Doppler frequency ν and was located at azimuth $\phi = \tau\omega_s$, then uniformly spaced transmit pulses led to target samples at a range cell given by [1] I-(14), namely

$$s(nT_p;\underline{\alpha}) = \gamma\, g(nT_p-\tau)\, e^{j2\pi\nu nT_p} \tag{1}$$

where $g(t)$ is the two-way antenna voltage gain pattern and T_p is the uniform interpulse period. In the derivation of this target model, it was assumed that the transmitted pulses were narrow compared to the Doppler period and to antenna pattern variations. In other words, the physical sampling was done by modulating a continuous phenomenon by a train of sampling pulses. A useful idealization is to represent the sampled data sequence as the continuous time function as follows:

$$\hat{s}(t;\underline{\alpha}) = s(t;\underline{\alpha}) \sum_{n=-\infty}^{\infty} \delta(t-nT_p) \tag{2}$$

where

$$s(t;\underline{\alpha}) = \gamma\, g(t-\tau)\, e^{j2\pi\nu t} \tag{3}$$

Then the Z-Transform of the uniformly sampled sequence is related to the Fourier Transform as follows:

---

[1] The notation I-(14) refers to equation (14) in Part I.

$$Z_s(e^{j2\pi fT_p};\underline{\alpha}) \triangleq Z\,[s(nT_p;\underline{\alpha})]\,\Big|_{z\,=\,e^{j2\pi fT_p}}$$

$$= F[\hat{s}(t;\underline{\alpha})] = \frac{1}{T_p}\sum_{n=-\infty}^{\infty} S(f - \frac{n}{T_p};\underline{\alpha}) \qquad (4)$$

where

$$S(f;\underline{\alpha}) = F\,[s(t;\underline{\alpha})] \qquad (5)$$

Equation (4) shows the foldover of the target spectrum every $1/T_p$ Hz.

When a two-pulse staggered PRF sampling pattern is used, samples of the target environment are taken at times 0, $\pm\,(T_p - \varepsilon)$, $\pm\,2T_p$, $\pm\,(3T_p - \varepsilon)$, $\pm\,4\,T_p$, ..., as shown in Figure 2. In this case, the sequence of samples has values

$$\ldots\ s(o), s(T_p-\varepsilon), s(2T_p), s(3T_p-\varepsilon), s(4T_p),\ \ldots \qquad (6)$$

These numbers correspond to sampling s(t) at times ... 0, $2T_p$, $4T_p$, $6T_p$, ..., and sampling $s(t-\varepsilon)$ at times ... T_p, $3T_p$, $5T_p$, $7T_p$, ···. A continucus time representation of the sampled-data waveform for the two-pulse staggered algorithm is therefore:

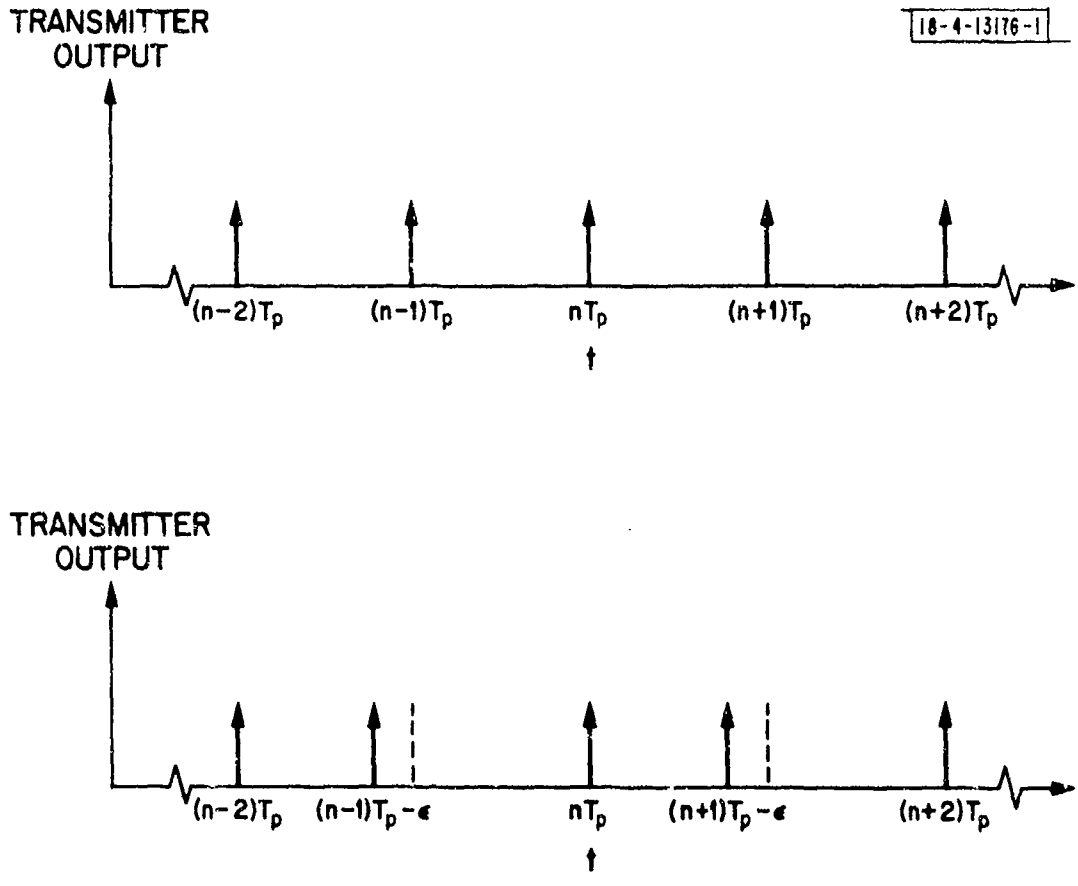

Fig. 2. Two-pulse staggered sampling pattern.

$$\hat{s}(t;\underline{\alpha}) = s(t;\underline{\alpha}) \sum_{n=-\infty}^{\infty} \delta(t-2nT_p) + s(t-\varepsilon;\underline{\alpha}) \sum_{n=-\infty}^{\infty} \delta[t-(2n-1)T_p] \qquad (7)$$

For the M-pulse stagger sampling pattern,

$s(t)$ is sampled at $0, MT_p, 2MT_p, \ldots$

$s(t-\varepsilon_1)$ is sampled at $T_p, (M+1)T_p, (2M+1)T_p, \ldots$

$s(t-\varepsilon_2)$ is sampled at $2T_p, (M+2)T_p, (2M+2)T_p, \ldots$

.

.

.

$s(t-\varepsilon_{M-1})$ is sampled at $(M-1)T_p, (2M-1)T_p, (3M-1)T_p, \ldots$ (8)

from which it is possible to deduce the following continuous time representation of the sampled-data waveform:

$$\hat{s}(t;\underline{\alpha}) = \sum_{m=0}^{M-1} \left| s(t-\varepsilon_m;\underline{\alpha}) \sum_{n=-\infty}^{\infty} \delta[t-(nM+m)T_p] \right| \qquad (9)$$

The Fourier Transform of this function is[2]:

$$\hat{S}(f;\underline{\alpha}) = \sum_{m=0}^{M-1} \left| e^{-j2\pi f\varepsilon_m} S(f;\underline{\alpha}) * \left[\frac{1}{MT_p} \sum_{n=\infty}^{\infty} e^{j2\pi fmT_p} \delta\left(f - \frac{n}{MT_p}\right) \right] \right| \qquad (10)$$

[2] The asterisk will denote convolution.

Use will be made of the following identity

$$\sum_{n=-\infty}^{\infty} e^{j2\pi fmT_p}\,\delta\left(f-\frac{n}{MT_p}\right) = \sum_{i=-\infty}^{\infty}\sum_{k=0}^{M-1} e^{j2\pi fmT_p}\,\delta\left(f-\frac{iM-k}{MT_p}\right)$$

$$= \sum_{i=-\infty}^{\infty}\sum_{k=0}^{M-1} e^{j2\pi\frac{iM-k}{MT_p}mT_p}\,\delta\left(f-\frac{iM-k}{MT_p}\right)$$

$$= \sum_{i=-\infty}^{\infty}\sum_{k=0}^{M-1} e^{-j2\pi\frac{km}{M}}\,\delta\left(f-\frac{iM-k}{MT_p}\right) \qquad (11)$$

In addition, for the target signal of interest

$$S(f;\underline{\alpha}) = \gamma' F_g(f-\nu)\, e^{-j2\pi f\tau} \qquad (12)$$

where $F_g(f)$ is the Fourier Transform of $g(t)$ and $\gamma' = \gamma\, e^{j2\pi\nu\tau}$. Using (12) and (11) in (10), the target spectrum becomes

$$\hat{S}(f;\underline{\alpha})$$

$$= \gamma'\sum_{m=0}^{M-1}\left\{F_g(f-\nu)\, e^{-j2\pi f(\tau+\varepsilon_m)} * \left[\frac{1}{MT_p}\sum_{i=-\infty}^{\infty}\sum_{k=0}^{M-1} e^{-j2\pi\frac{km}{M}}\,\delta\left(f-\frac{iM-k}{MT_p}\right)\right.\right.$$

$$\left.\left. = \frac{\gamma'}{T_p}\sum_{i=-\infty}^{\infty}\frac{1}{M}\sum_{k=0}^{M-1}\sum_{m=0}^{M-1} e^{-j2\pi\frac{km}{M}}\, e^{-j2\pi\left(f+\frac{k}{MT_p}-\frac{i}{T_p}\right)(\tau+\varepsilon_m)} F_g\left(f-\nu+\frac{k}{MT_p}-\frac{i}{T_p}\right)\right]\right\}$$

(13)

Since the target is sampled only at discrete instants, the delay parameter τ can be estimated only to within an interpulse period. Therefore, it can be assumed that

$$\tau = I(\tau)\, T_p \tag{14}$$

where $I(\tau)$ is some unknown integer. Then (13) becomes

$$\hat{S}(f;\underline{\alpha}) =$$

$$\frac{\gamma'}{T_p} e^{-j2\pi f\tau} \sum_{i=-\infty}^{\infty} \left\{ \sum_{k=0}^{M-1} e^{-j2\pi \frac{kI(\tau)}{M}} \left[\frac{1}{M} \sum_{m=0}^{M-1} e^{-j2\pi \frac{km}{M}} e^{-j2\pi (f+\frac{k}{MT_p} - \frac{i}{T_p})\varepsilon_m} F_g(f-\nu+\frac{k}{MT_p} - \frac{i}{T_p}) \right] \right\} \tag{15}$$

Since the term $e^{-j2\pi f\varepsilon_m}$ changes slowly relative to the width of the function $F_g(f-\nu)$, then to a good approximation

$$e^{-j2\pi f\varepsilon_m} F_g(f-\nu) \simeq e^{-j2\pi\nu\varepsilon_m} F_g(f-\nu) \tag{16}$$

and (15) can be written as

$$\hat{S}(f;\underline{\alpha}) =$$

$$\frac{\gamma'}{T_p} e^{-j2\pi f\tau} \sum_{i=-\infty}^{\infty} \left\{ \sum_{k=0}^{M-1} e^{-j2\pi \frac{kI(\tau)}{M}} \left[\frac{1}{M} \sum_{m=0}^{M-1} e^{-j2\pi \frac{km}{M}} e^{-j2\pi\nu\varepsilon_m} \right] F_g(f-\nu + \frac{k}{MT_p} - \frac{i}{T_p}) \right\} \tag{17}$$

It is appropriate to define the coefficients

$$a_k(\tau) = e^{-j2\pi \frac{kI(\tau)}{M}} \tag{18a}$$

$$b_k(\nu) = \frac{1}{M} \sum_{m=0}^{M-1} e^{-j2\pi \frac{km}{M}} e^{-j2\pi\nu\varepsilon_m} \tag{18b}$$

$$c_k(\tau,\nu) = a_k(\tau) b_k(\nu) \tag{18c}$$

$$k = 0, 1, \cdots, M-1$$

as this leads to the following convenient expression for the Z-Transform of the target:

$$Z_s\left(e^{j2\pi f T_p}; \underline{\alpha}\right) = \gamma' e^{-j2\pi f\tau} \left\{ \frac{1}{T_p} \sum_{i=-\infty}^{\infty} \left[\sum_{k=0}^{M-1} c_k(\tau,\nu) F_g\left(f - \nu + \frac{k}{MT_p} - \frac{i}{T_p}\right) \right] \right\} \tag{19}$$

Clutter Model

In Section II of Part I, it was shown that each clutter scattering center could be treated as a point target having zero Doppler. Therefore, as in I-(15), the n^{th} scatterer at azimuth ϕ_n in the particular ring of interest generates the clutter signal return

$$c(t_k) = \gamma_n\, g(t_k - \tau_n) \tag{20}$$

where $\tau_n = \phi_n/\omega_s - m\Delta T/2$, $\gamma_n = A_n e^{j\theta_n}$ and t_n represents the times the samples are taken. As before, A_n is related to the scattering cross-section of the n^{th} scatterer and θ_n the carrier phase it introduces. From scan-to-scan, the shift in transmitter phase and the jitter in the antenna rotation render θ_n and A_n random variables, but over any one scan, (20) represents a deterministic signal return. Hence, the analysis used to derive the Fourier Transform of the non-uniformly sampled target return is directly applicable to (20). The using (15) the transform is

$$\hat{C}_n(f) =$$

$$\frac{\gamma_n}{T_p} e^{-j2\pi f\tau_n} \sum_{i=-\infty}^{\infty} \left\{ \sum_{k=0}^{M-1} e^{-j2\pi \frac{kI(\tau_n)}{M}} \left[\frac{1}{M} \sum_{m=0}^{M-1} e^{-j2\pi\frac{km}{M}} e^{-j2\pi(f+\frac{k}{MT_p} - \frac{i}{T_p})\varepsilon_m} F_g(f+\frac{k}{MT_p} - \frac{i}{T_p}) \right] \right\} \tag{21}$$

Equation (21) is derived from (15) rather than (19) because the latter equation has made use of the approximation in (16). Since clutter returns can be orders of magnitude greater than the signal returns, approximations cannot be made unless they can be justified on the basis of signal-to-clutter ratios. The total clutter return is due to a finite number of scatterers, hence

$$C(t_k) = \sum_n C_n(t_k) \tag{22}$$

and the Fourier Transform of this aggregate of returns is

$$\hat{C}(f) = \sum_{n} \hat{C}_n(f) \tag{23}$$

Therefore, the energy spectral density of the clutter measured over a single scan is

$$\left|\hat{C}(f)\right|^2 = \sum_{n_1} \sum_{n_2} \hat{C}_{n_1}(f)\, \hat{C}^{*}_{n_2}(f) \tag{24}$$

This is a random process in the sense that after each scan the values of A_n and θ_n change in a random fashion. Then the average <u>power</u> spectral density of the clutter is

$$S_c(f) = \frac{1}{T_s} \overline{\left|\hat{C}(f)\right|^2} = \frac{1}{T_s} \sum_{n_1} \sum_{n_2} \overline{C_{n_1}(f)\, C^{*}_{n_2}(f)} \tag{25}$$

where T_s is the scan time and the bar denotes statistical averaging over the random variables A_n and θ_n.

Since the amplitudes, phases and azimuthal locations of the scatterers are independent, each of the random variables in (25) can be averaged separately. Furthermore, it follows that

$$\overline{Y_{n_1} Y^{*}_{n_2}} = \overline{\left|Y_{n_1}\right|^2}\ \delta_{n_1, n_2} \tag{26}$$

and since the frequency extent of $F_g(f)$ is narrow relative to a separation k/MTp,

$$F_g(f + \frac{k_1}{MT_p} - \frac{i_1}{T_p})\, F_g^*(f + \frac{k_2}{T_p} - \frac{i_2}{T_p}) \simeq \left|F_g(f + \frac{k_1}{MT_p} - \frac{i_1}{T_p})\right|^2 \delta_{k_1,k_2} \delta_{i_1,i_2} \tag{27}$$

Substituting (21) in (25) and using (26) and (27), it follows that

$$S_c(f) = \frac{1}{T_s}\left(\sum_n |\gamma_n|^2\right)\frac{1}{T_p^2} \sum_{i=-\infty}^{\infty} \left\{\sum_{k=0}^{M-1} \left| \frac{1}{M} \sum_{m=0}^{M-1} e^{-2\pi \frac{km}{M}} A_m(f + \frac{k}{MT_p} - \frac{i}{T_p})\right|^2\right\} \tag{28}$$

where

$$A_m(f) = e^{-j2\pi f \epsilon_m} F_g(f) \tag{29}$$

In (29), $1/\epsilon_m$ is generally much greater than the frequency extent of the clutter and it is reasonable to assume that

$$e^{-j2\pi f \epsilon_m} F_g(f) \simeq F_g(f) \tag{30}$$

Since the clutter signals can be many orders of magnitude greater than the signal, this approximation must be undertaken with care in each application. An example of the analysis needed to justify (30) is given in a later para-

graph for the two-pulse staggered case. Assuming that this approximation is valid then the average power spectrum of the clutter process can be written as:

$$S_c(f) = \frac{\sigma^2}{T_s} \cdot \frac{1}{T_p^2} \cdot \sum_{i=-\infty}^{\infty} \left\{ \sum_{k=0}^{M-1} \left[\left| \frac{1}{M} \sum_{m=0}^{M-1} e^{-j2\pi \frac{km}{M}} \right|^2 \left| F_g\left(f + \frac{k}{MT_p} - \frac{i}{T_p}\right) \right|^2 \right] \right\} \tag{31}$$

where

$$\sigma^2 = \sum_n \overline{|\gamma_n|^2} \tag{32}$$

denotes the average clutter power per range ring. It is shown in the Appendix that

$$\frac{1}{M} \sum_{m=0}^{M-1} e^{-j2\pi \frac{km}{M}} = \delta_{k,0} \tag{33}$$

hence, the clutter spectrum reduces to

$$S_c(f) = \frac{\sigma^2}{T_s} \cdot \frac{1}{T_p^2} \cdot \sum_{i=-\infty}^{\infty} \left| F_g\left(f - \frac{i}{T_p}\right) \right|^2 \tag{34}$$

Receiver Noise Model

It follows directly from I-(36) that staggering the transmitter PRF has no effect on the receiver noise process. Therefore, it remains a zero-mean white noise process with spectral dersity $2N_0$.

Two-Pulse Staggering

In order to gain some physical understanding of the mathematical expressions for the target and clutter spectra the special case of a two-pulse stagger will be studied. This is illustrated in Figure 2. Using M = 2, $\varepsilon_0 = 0$, $\varepsilon_1 = \varepsilon$ in (18) and (19) the transform of the target signal is

$$\hat{S}(f;\underline{\alpha}) = \gamma' e^{-j2\pi f\tau} \left\{ \frac{1}{T_p} \sum_{i=-\infty}^{\infty} \left[C_0(\tau,\nu) F_g(f - \nu - \frac{i}{T_p}) + C_1(\tau,\nu) F_g(f - \nu + \frac{1}{2T_p} - \frac{i}{T_p}) \right] \right\} \tag{35}$$

where

$$C_0(\tau,\nu) = (1 + e^{-j2\pi\nu\varepsilon})/2 \tag{36a}$$

$$C_1(\tau,\nu) = (-1)^{I(\tau)} (1 - e^{-j2\pi\nu\varepsilon})/2 \tag{36b}$$

Hence the spectrum of the target return is

$$\left|\hat{S}(f;\underline{\alpha})\right|^2 = \frac{|\gamma'|^2}{T_p^2} \sum_{i=-\infty}^{\infty} \left[(\cos^2 \pi\nu\varepsilon) \left| F_g(f - \nu - \frac{i}{T_p}) \right|^2 + (\sin^2 \pi\nu\varepsilon) \left| F_g(f - \nu + \frac{1}{2T_p} - \frac{i}{T_p}) \right|^2 \right] \tag{37}$$

Typical plots of the target spectrum are illustrated in Figure 3. There are two significant observations to be made: (1) whereas in the uniformly sampled case all of target energy is located at PRF multiples of the true Doppler, staggering causes the energy to be split into two pieces separated by one-half

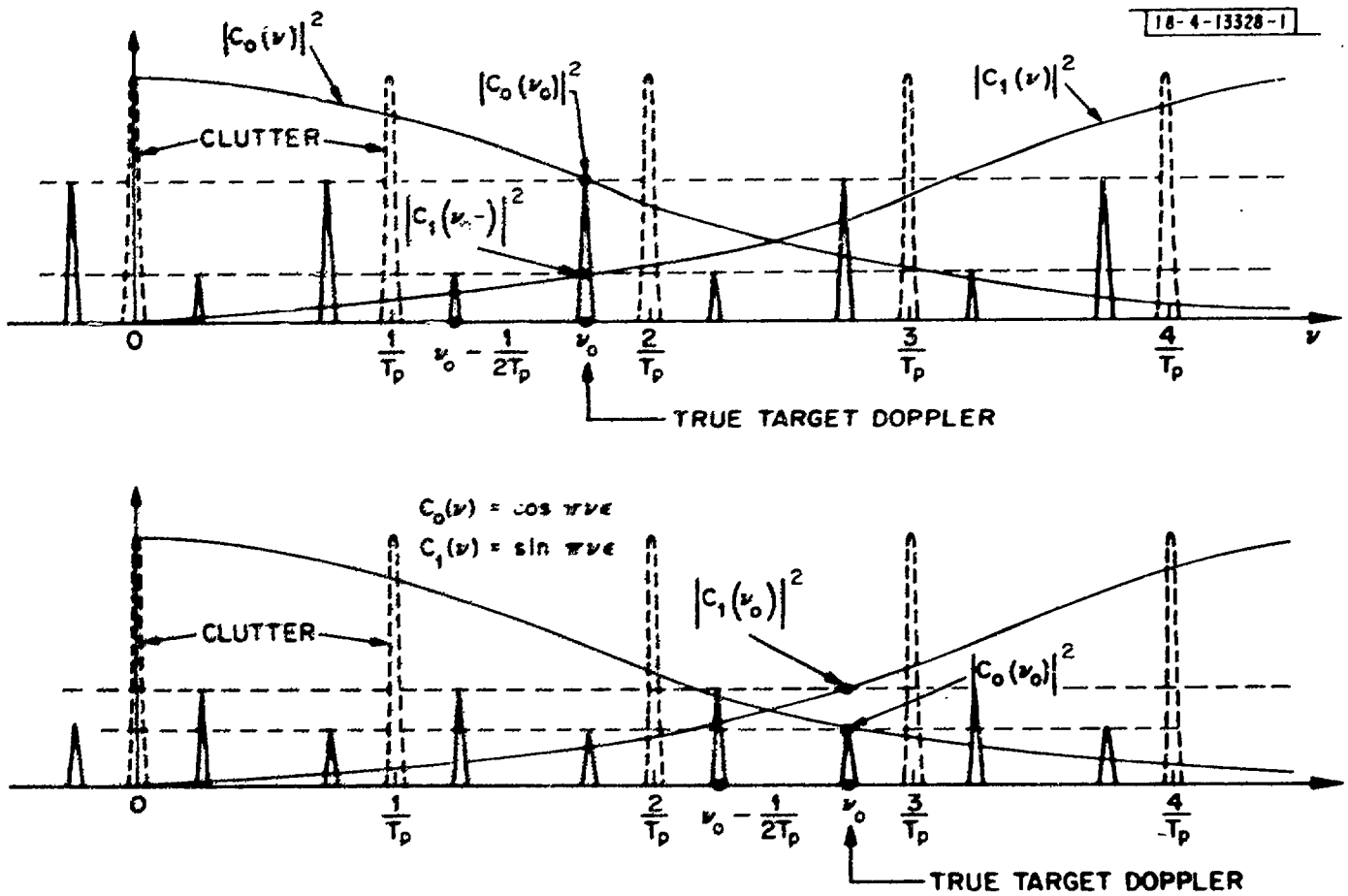

Fig. 3. Typical target spectra for two-pulse stagger.

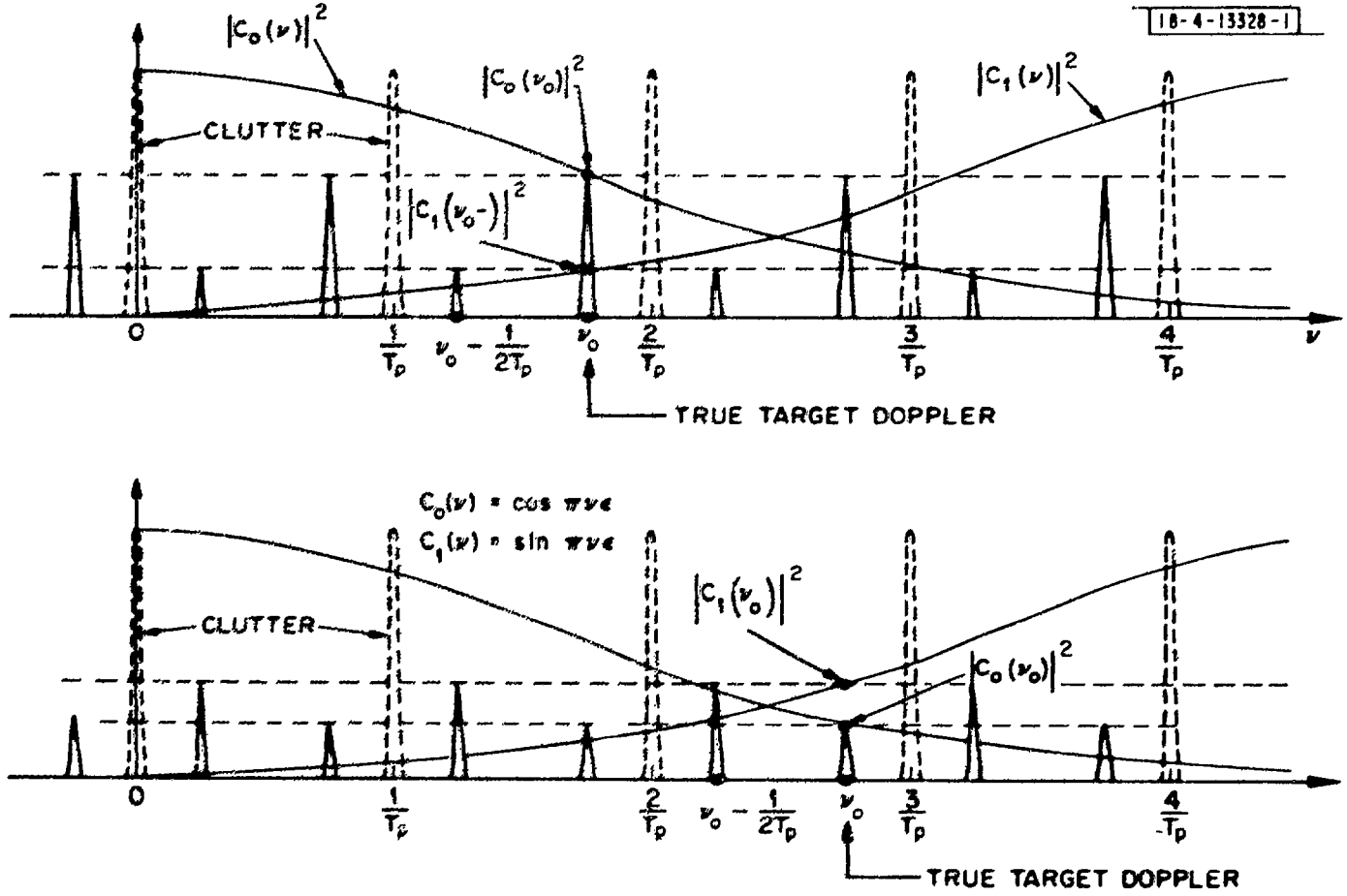

Fig. 3. Typical target spectra for two-pulse stagger.

the PRF, and the pair folds over at the PRF, and (2) whereas in the uniformly sampled case targets moving at dopplers greater than a PRF led to spectra that were indistinguishable, now the fundamental ambiguity occurs with a period $2/\epsilon$. This shows that staggered PRF's provide a basis for unambiguous velocity estimation.

From (31), the exact form of the clutter spectrum reduces to

$$S_c(f) = \frac{\sigma^2}{T_s} \cdot \frac{1}{T_p^2} \cdot \sum_{i=-\infty}^{\infty} \left[\cos^2\pi(f - \frac{i}{T_p})\epsilon\right] \left|F_g(f - \frac{i}{T_p})\right|^2$$

$$+ \left[\sin^2\pi(f + \frac{1}{2T_p} - \frac{i}{T_p})\epsilon\right] \left|F_g(f + \frac{1}{2T_p} - \frac{i}{T_p})\right|^2 \qquad (38)$$

Since the frequency extent of $F_g(f)$ is very narrow relative to $1/T_p$, it can reasonably be assumed that

$$(\cos^2\pi f\epsilon)\left|F_g(f)\right|^2 \approx \left|F_g(f)\right|^2 \qquad (39a)$$

$$(\sin^2\pi f\epsilon)\left|F_g(f)\right|^2 \approx (\pi f\epsilon)^2 \left|F_g(f)\right|^2 \qquad (39b)$$

Using these approximations the clutter spectra can be sketched as shown in Figure 4 from which it is observed that as for the target spectrum the clutter power also splits into two pieces, one piece being located at DC, the other at $-1/2\ T_p$, with the aggregate folding over at the PRF. The simple sketch

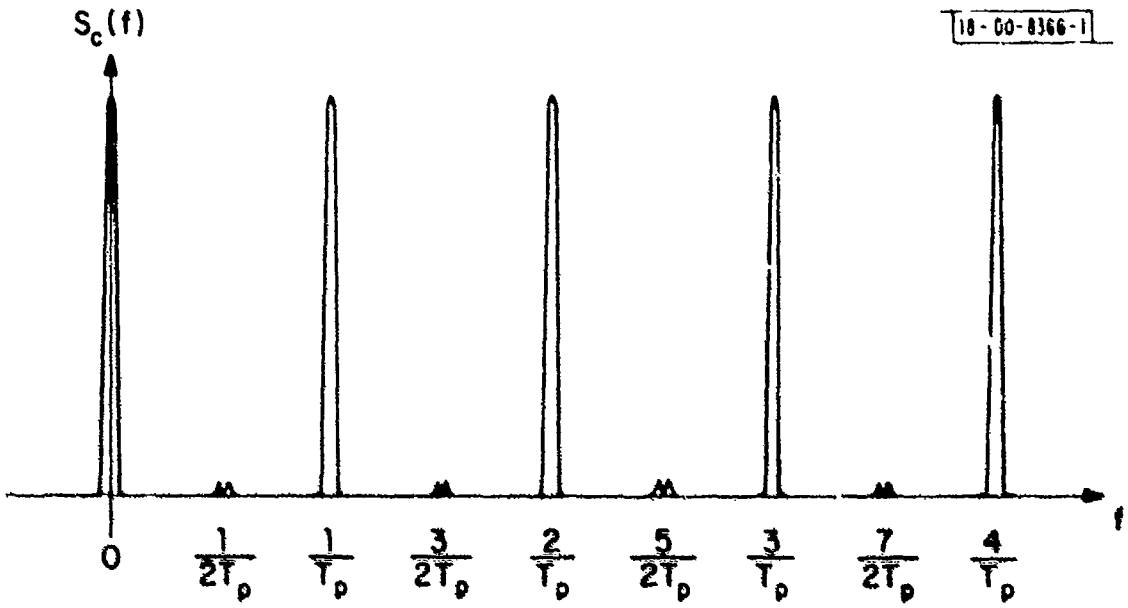

Fig. 4. Typical clutter spectral density for two-pulse stagger.

has been drawn to indicate that the clutter power at 1/2 T_p is significantly smaller than that at DC. A quantitative measure of the relative power in each of these terms can be found by integrating (39a) and (39b). This has been done for the sin x/x antenna pattern and ARSR system parameters and it was found that the clutter power at 1/2 T_p is 56 dB down from that at DC. Since 10 bit A/D converters correspond to a subclutter visibility no greater than 40 dB, the effect of the clutter power at 1/2 T_p is negligible, hence justifying the assumptions leading to the clutter spectrum in (34).

Therefore, the implications of the staggered PRF are now clear: Whereas the energy of a moving target return splits into two pieces, the clutter power continues to fold over at multiples of $1/T_p$. Hence, if the target Doppler is also a multiple of $1/T_p$, namely a former blind speed, then although one portion of the target energy is masked by the DC clutter, the other portion is located in a relatively clutter-free area at 1/2 T_p. This is the reason staggered PRF enhances target detection. However, if in addition, filters that are matched to the target spectrum are constructed, then it appears that Doppler estimation over a frequency interval larger than one PRF is possible. Although the topic is discussed in more detail in Section IV we briefly discuss the implementation of the filter matched to the two-pulse staggered signal spectrum.

Matched Filter Realization

From the preceding discussion it is shown that the target spectrum is a unique function of the true target Doppler over an interval that can be

many times larger than the PRF. If a matched filter bank could be constructed then not only would the detection performance be optimized but unambiguous estimation of target Doppler would be possible.

Let us suppose that we require the resolution of velocity to within the interval $\Delta v = 1/NT_p$. Then each PRF interval can be quantized into N subintervals and we can then express the true target Doppler as

$$v = \frac{i_o}{T_p} + \frac{n_o}{NT_p} \quad .$$

From (35) the signal spectrum for the two-pulse stagger is

$$\hat{S}(f;\underline{\alpha}) = \gamma \sum_{i=-\infty}^{\infty} \left[C_0(\tau,v) F_g\left(f - \frac{n_o}{NT_p} - \frac{i-i_o}{T_p}\right) + C_1(\tau,v) F_g\left(f - \frac{n_o}{NT_p} - \frac{i-i_o}{T_p} + \frac{1}{2T_p}\right) \right]$$

The infinite sum shows the periodic foldover of the target spectrum at the PRF. From a measurements point of view, nature allows us to observe this function only in the interval $[0, 1/T_p]$. Then we see only the function

$$\hat{S}(f;\underline{\alpha}) = \gamma \left[C_0(\tau,v) F_g\left(f - \frac{n_o}{NT_p}\right) + C_1(\tau,v) F_g\left(f - \frac{n_o}{NT_p} + \frac{1}{2T_p}\right) \right]$$

We can readily construct a bank of filters that extend over the $[0, 1/T_p]$

range where each filter is tuned to the function $F_g^*(f - \frac{n}{NT_p})$, $n=0,1,\ldots,N-1$. By themselves, these are not matched to the specified signal. To accomplish this, we combine weighted pairs of filters that are separated by $1/2T_p$ Hz. For the filters tuned to n/NT_p and $(n-1/2)/NT_p$ we apply the weights $C_o^*(\tau, \frac{i}{T_p} + \frac{n}{NT_p})$, $C_1^*(\tau, \frac{i}{T_p} + \frac{n}{NT_p})$ for $i=0,\pm1,\pm2,\ldots,\pm M$. For each value of i, this gives rise to another filter with transfer function

$$H_{i,n}(f) = C_o^*(\tau; \frac{i}{T_p} + \frac{n}{NT_p})F_g^*(f - \frac{n}{NT_p})$$

$$+ C_1^*(\tau; \frac{i}{T_p} + \frac{n}{NT_p})F_g^*(f - \frac{n}{NT_p} = \frac{1}{2T_p})$$

$$i=o,\pm,\ldots, \pm M,\ n=0,1,\ldots,N-1$$

When $i=i_o$, $n=n_o$, this filter is matched to the two-pulse staggered signal.

From a practical point of view, the sub-bank of filters $\left\{F_g^*(f - \frac{n}{NT_p})\right\}_{n=0}^{N-1}$ can be formed by taking an N-point Discrete Fourier Transform (DFT) of the received signal. The super-bank of filters is then obtained by multiplying the n^{th} DFT coefficient by $C_o^*(\tau; \frac{i}{T_p} + \frac{n}{NT_p})$ and the $(n - \frac{N}{2})^{th}$ DFT coefficient by $C_1^*(\tau; \frac{i}{T_p} + \frac{n}{NT_p})$ for $i=0, \pm1,\ldots, \pm M$. Therefore, an N-point DFT gives rise to a bank of 2MN matched filters that extend over the frequency interval $\left[-\frac{M}{T_p}, \frac{M}{T_p}\right]$ simply by combining the outputs of the DFT coefficients in the right way.

In Section IV we return to this discussion in more detail when we consider the MTI ambiguity function. In Section III, a quantitative measure of the improvement in detection performance will be evaluated using the Signal-to-Interference Ratio (SIR) that was derived in Part I.

III. SIR PERFORMANCE ANALYSIS FOR STAGGERED PRF

The SIR for an arbitrary linear, sampled-data filter when sampled at time τ was given by I-(72), viz.

$$\rho(\tau) = T_p \frac{\left| \int_{-1/2T_p}^{1/2T_p} H(e^{j2\pi fT_p}) Z_s(e^{j2\pi fT_p}; \underline{a}_0)(e^{j2\pi f\tau})\, df \right|^2}{\int_{-1/2T_p}^{1/2T_p} \left|H(e^{j2\pi fT_p})\right|^2 \left[S_c(e^{j2\pi fT_p}) + 2N_0\right] df} \tag{40}$$

Even though the transmitter PRF is staggered, the sampled-data processor operates on the samples of the signal and noise and it matters not when those samples were taken. Therefore, (40) applies to the present problem, although it is noted that the signal spectrum will be different, due to the non-uniform sampling. As before, it is noted that only those frequency terms in the interval $(-1/2T_p, 1/2T_p)$ are of interest. This is consistent with (19) since the frequency dependence shows up only in terms like $F_g(f-\nu + \frac{k}{MT_p} - \frac{i}{T_p})$ which is folded over every $1/T_p$ hz.

Using the Schwarz inequality it is easy to show that (40) is maximized by choosing

$$H(e^{j2\pi fT_p}) = \frac{Z_s^*(e^{j2\pi fT_p}; \underline{a}_0)}{S_c(e^{j2\pi fT_p}) + 2N_0} \tag{41}$$

which is the clutter filter, matched filter cascade combination. When this is done, the resulting maximum value of the SIR is

$$\rho_{opt} = T_p \int_{-1/2T_p}^{1/2T_p} \frac{\left|Z_s(e^{j2\pi fT_p};\underline{\alpha}_o)\right|^2}{S_c(e^{j2\pi fT_p}) + 2N_o} \, df \tag{42}$$

The aliased clutter spectrum is given by (34), but since the integration extends over the $(-1/2T_p, 1/2T_p)$ frequency interval, only the term about DC need be taken. Taking the squared magnitude of (19) and using the approximation in (27), the target spectral density reduces to

$$\left|Z_s(e^{j2\pi fT_p};\underline{\alpha}_o)\right|^2 = \frac{|Y_o|^2}{T_p^2} \sum_{i=-\infty}^{\infty} \sum_{k=0}^{M-1} \left|c_k(\tau_o,\nu_o)\right|^2 \left|F_g(f - \nu_o + \frac{k}{MT_p} - \frac{i}{T_p})\right|^2 \tag{43}$$

Using these results and the fact that

$$\left|c_k(\tau,\nu)\right| = \left|a_k(\tau)b_k(\nu)\right| = \left|b_k(\nu)\right| \tag{44}$$

which follows from (18), then the SIR in (42) becomes

$$\rho_{opt}(\nu_o) = \left|Y_o\right|^2 \sum_{k=0}^{M-1} \left|b_k(\nu_o)\right|^2 \int_{-1/2T_p}^{1/2T_p} \frac{\sum_{i=-\infty}^{\infty} \left|F_g(f - \nu_o + \frac{k}{MT_p} - \frac{i}{T_p})\right|^2}{\frac{\sigma_s^2}{T_s} \cdot \frac{1}{T_p} \cdot \left|F_g(f)\right|^2 + 2N_oT_p} \, df \tag{45}$$

Rather than attempt a rigorous evaluation of (45), it is easier to draw upon the physical understanding of the target and clutter spectra to simplify the SIR expression. It was shown in the last section that the M-pulse staggered PRF causes the target energy to split into M components that are folded over into the $(-1/2T_p, 1/2T_p)$ interval, while the clutter was distributed about DC. Since the frequency extent of $F_g(f)$ is narrow relative to the window $1/MT_p$, there are values of ν_o for which there is no interaction between the clutter and target spectra. In this case, for each ν_o there is a value of i that puts $F_g(f - \nu_o + \frac{k}{MT_p} - \frac{i}{T_p})$ within the $(-1/2T_p, 1/2T_p)$ interval and

$$\int_{-1/2T_p}^{1/2T_p} \frac{\sum_{i=-\infty}^{\infty} \left|F_g(f - \nu_o + \frac{k}{MT_p} - \frac{i}{T_p})\right|^2}{\frac{\sigma^2}{f_s} \cdot \frac{1}{T_p}\left|F_g(f)\right|^2 + 2N_o T_p} df = \frac{1}{2N_o T_p} \int_{-1/2T_p}^{1/2T_p} \left|F_g(f - \nu_o + \frac{k}{MT_p} - \frac{i}{T_p})\right|^2 df$$

$$= \frac{E_g}{2N_o T_p} \tag{46}$$

where

$$E_g = \int_{-1/2T_p}^{1/2T_p} \left|F_g(f)\right|^2 df \tag{47}$$

In the Appendix it is shown that

$$\left|\sum_{k=0}^{M-1} b_k(\nu_o)\right|^2 = 1 \tag{48}$$

whence it follows that

$$\rho_{opt}\,(\nu_o) = \frac{|\gamma_o|^2 E_g}{2N_o T_p} \tag{49}$$

This is, of course, just the coherent integration gain provided by matched filtering the target out of the white noise background.

The SIR degrades from this optimum value when any one of the M components of the target spectrum interacts with the clutter spectra. The worst case occurs when, for some k and i, k_o and i_o say,

$$-\nu_o + \frac{k_o}{MT_p} - \frac{i_o}{T_p} = 0 \tag{50}$$

In this case, since the clutter-to-white noise ratio is very large,

$$\int_{-1/2T_p}^{1/2T_p} \frac{\left|F_g(f - \nu_o + \frac{k_o}{MT_p} - \frac{i_o}{T_p})\right|^2}{\frac{\sigma^2}{T_s}\left|F_g(f)\right|^2 + 2N_o T_p} = \frac{T_s}{\sigma^2} \tag{51}$$

For the remaining M-1 components of the target spectrum that are located within the $(-1/2T_p, 1/2T_p)$ interval, there is little interaction with the clutter spectra. Hence, for those values of $k \neq k_o$ (46) holds and the SIR

can be written as

$$\rho_{opt}(\nu_o) = |\gamma_o|^2\left[\frac{E_g}{2N_oT_p}\sum_{\substack{k=0\\k\neq k_o}}^{M-1}|b_k(\nu_o)|^2 + \frac{T_s}{\sigma^2}|b_{k_o}(\nu_o)|^2\right]$$

$$= \frac{|\gamma_o|^2E_g}{2N_oT_p}\left\{1-|b_{k_o}(\nu_o)|^2\left[1-\frac{2N_oT_pT_s}{\sigma^2E_g}\right]\right\} \qquad (52)$$

$$\approx \frac{|\gamma_o|^2E_g}{2N_oT_p}\left[1-|b_{k_o}(\nu_o)|^2\right]$$

where the last approximation follows from the fact that the clutter to receiver noise ratio is >> 1. This expression for the SIR holds for values of ν_o given by

$$\nu_o = \frac{k_o}{MT_p} + \frac{m_o}{T_p} \qquad (53)$$

where first a value of m_o is chosen and then for each m_o, $k_o = 0,1,2,\cdots,M-1$. Then the optimum SIR performance curve can be sketched by using the formula

$$\frac{\rho(\nu_o)}{\left[\frac{|\gamma_o|^2E_g}{2N_oT_p}\right]} = \begin{cases} 1-|b_{k_o}(\nu_o)|^2 & \text{if } \nu_o = \frac{m_o}{T_p} + \frac{k_o}{MT_p} \\ 1 & \text{otherwise} \end{cases} \qquad (54)$$

For the case of a two-pulse stagger, $M = 2$, $k_o = 0$ or 1 and

$$|b_0(\nu_0)|^2 = \cos^2 \pi \nu_0 \varepsilon \tag{55a}$$

$$|b_1(\nu_0)|^2 = \sin^2 \pi \nu_0 \varepsilon \tag{55b}$$

so that

$$\frac{\rho(\nu_0)}{\left[\frac{|\gamma_0|^2 E_g}{2N_0 T_p}\right]} = \begin{cases} \sin^2 \pi \nu_0 \varepsilon & \text{if} \quad \nu_0 = \frac{m_o}{T_p} \\ \cos^2 \pi \nu_0 \varepsilon & \text{if} \quad \nu_0 = \frac{m_o}{T_p} + \frac{1}{2T_p} \\ 1 & \text{otherwise} \end{cases} \tag{56}$$

Whereas when no pulse staggering is used ($\varepsilon = 0$), the SIR is essentially zero at multiples of the PRF, staggered pulse transmissions lead to meaningful detection performance, especially at higher Doppler velocities. The price paid for this enhanced performance at the blind speeds is a degradation in the SIR performance at intermediate Doppler frequencies. These results are summarized in the SIR performance curve plotted in Figure 5. It is worth noting that similar results can be obtained for the pulse canceller clutter filters by working directly from (40) using the appropriate filter transfer functions. The SIR performance of the ASR-7 that uses a 6-pulse stagger algorithm is shown in Figure 6.

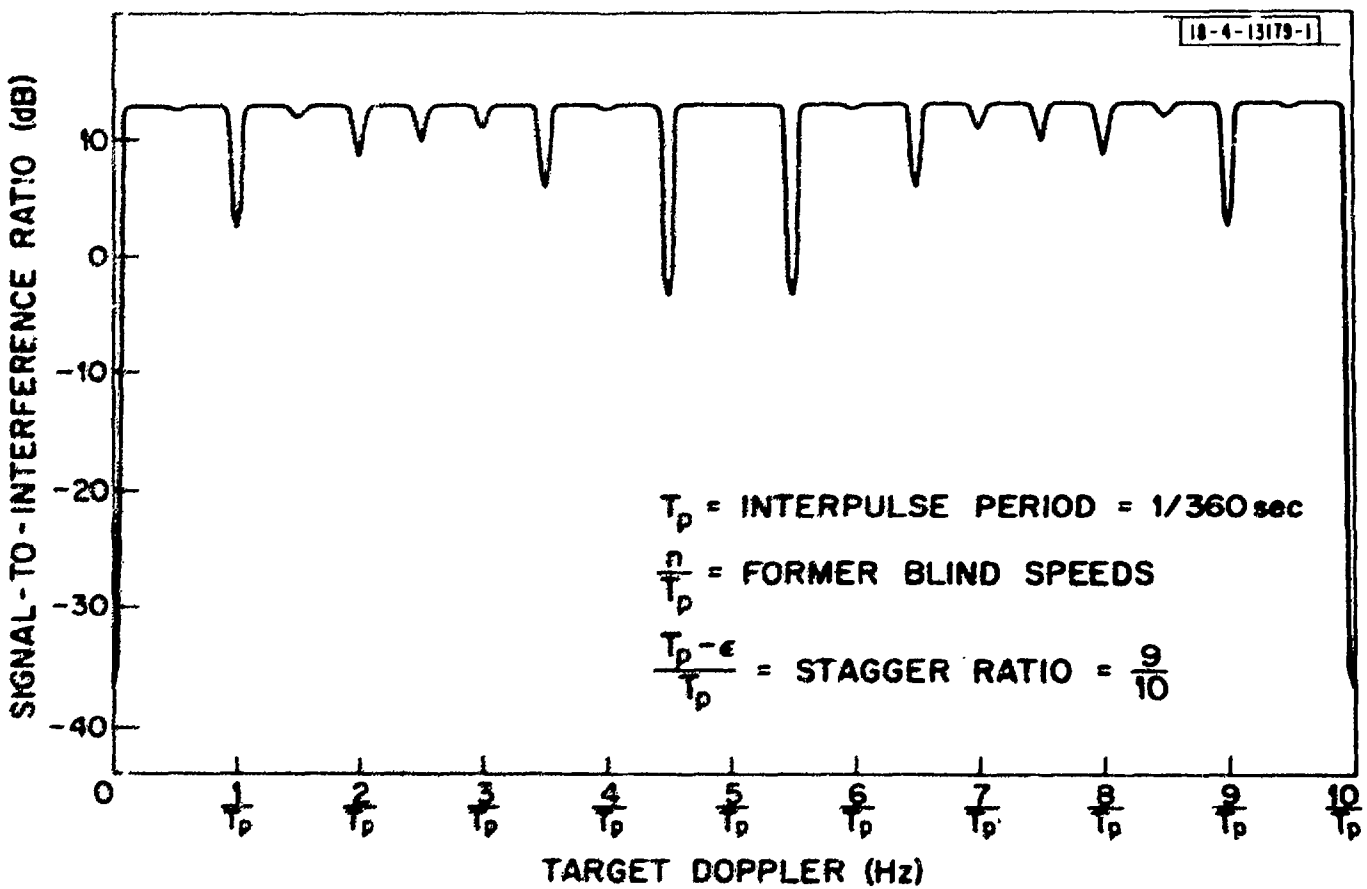

Fig. 5. Optimum SIR performance using two-pulse staggered PRF.

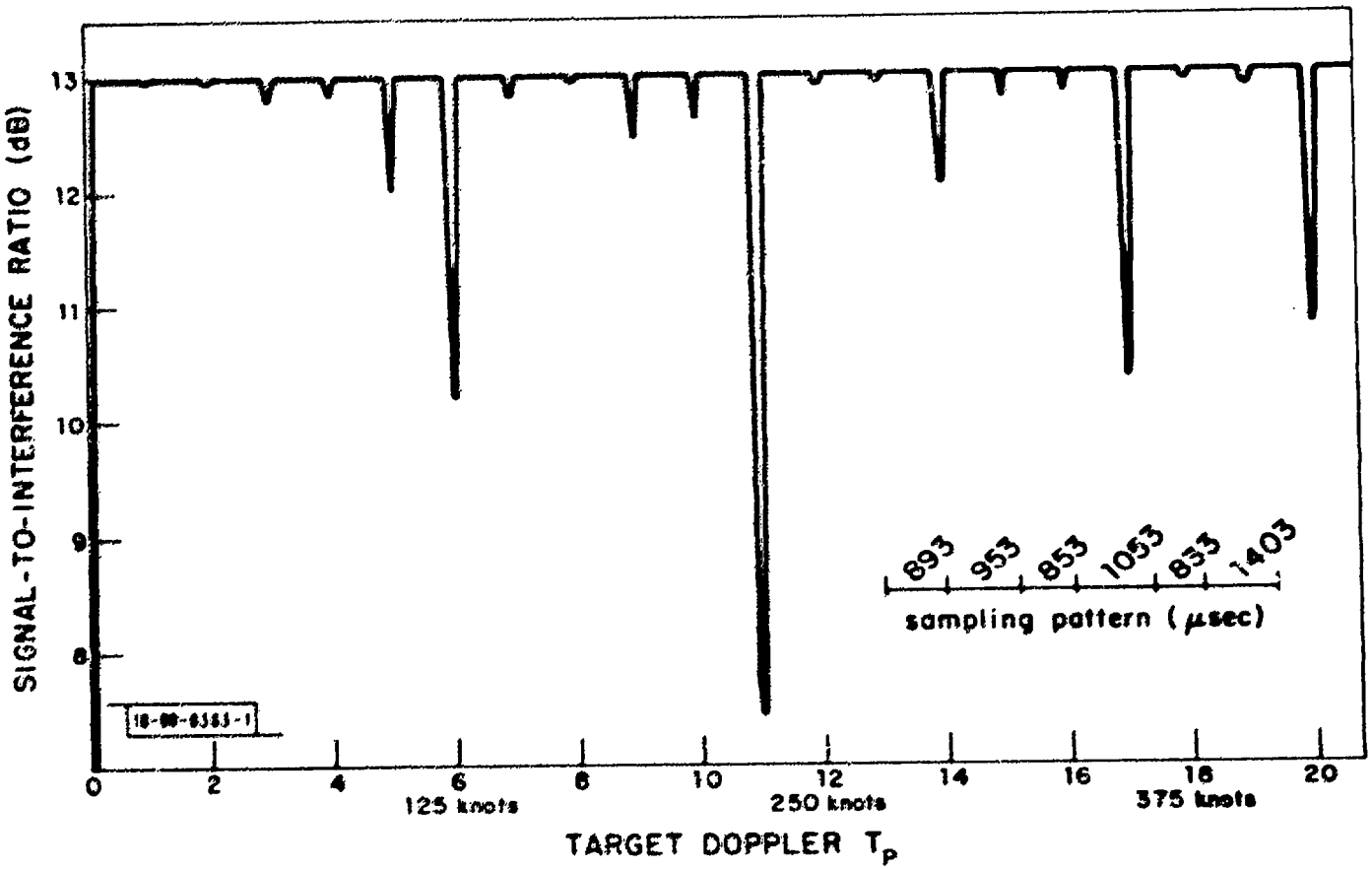

Fig. 6. Optimum ASR-7 performance using an operational six-pulse stagger.

IV. STAGGERED PRF AMBIGUITY FUNCTION

In Section II, the target spectrum resulting from a staggered PRF transmission sequence was derived and, for the two-pulse case, illustrated in Figure 3. It was noted that the spectra for targets separated by Doppler shifts greater than one PRF were not identical as was the case when uniform sampling was used. This indicates that it may well be possible to estimate target Doppler unambiguously. This question is most easily examined by evaluating the ambiguity function of the staggered PRF pulse train. The calculation is not conceptually difficult but it can become tedious. In order to develop some intuition, the clutter-free ambiguity function will be computed first and then generalized to the situation in which the clutter filter is present. In the former case the ambiguity function is the delay-Doppler distribution of the output of the matched filter. It is denoted by $|\xi(\underline{a},\underline{a}_0)|$ where

$$\xi(\underline{a},\underline{a}_0) = \int_{-1/2\,T_p}^{1/2\,T_p} Z_s^*(f;\underline{a})\, Z_s(f;\underline{a})\, df \qquad (57)$$

Rather than attempt to evaluate (57) by direct substitution it is easier and more instructive to draw heavily upon the physical interpretation of the correlation operation implied by this equation. The necessary intuition can be developed by studying the transmitted signal for the three-pulse staggered case. From (18) and (19) the transform of the target signal is

$$Z_s(f;\underline{\alpha}_0) = \frac{\gamma_0}{T_p} e^{-j2\pi f\tau_0} \sum_{i=-\infty}^{\infty} \Big[a_0(\tau_0) b_0(\nu_0) F_g(f - \nu_0 - \frac{i}{T_p})$$

$$+ a_1(\tau_0) b_1(\nu_0) F_g(f - \nu_0 + \frac{1}{3T_p} - \frac{i}{T_p})$$

$$+ a_2(\tau_0) b_2(\nu_0) F_g(f - \nu_0 + \frac{2}{3T_p} - \frac{i}{T_p}) \Big] \qquad (58)$$

The magnitude characteristic of this function is illustrated in Figure 7a. It will be assumed that τ, τ_0 and ν_0 are fixed so that the correlation operation in (57) can be studied as a function of ν. Making use of the $1/T_p$ periodicity in the target spectrum, the integral in (57) can be evaluated using

$$\xi(\tau, \tau_0, \nu, \nu_0) = \int_{\nu_0 - 1/T_p}^{\nu_0} Z_s^*(f; \tau, \nu)\, Z_s(f; \tau_0, \nu_0)\, df \qquad (59)$$

The first situation of interest occurs when $\nu = \nu_0$ in which case the Doppler coefficients line up exactly. Equation (59) becomes

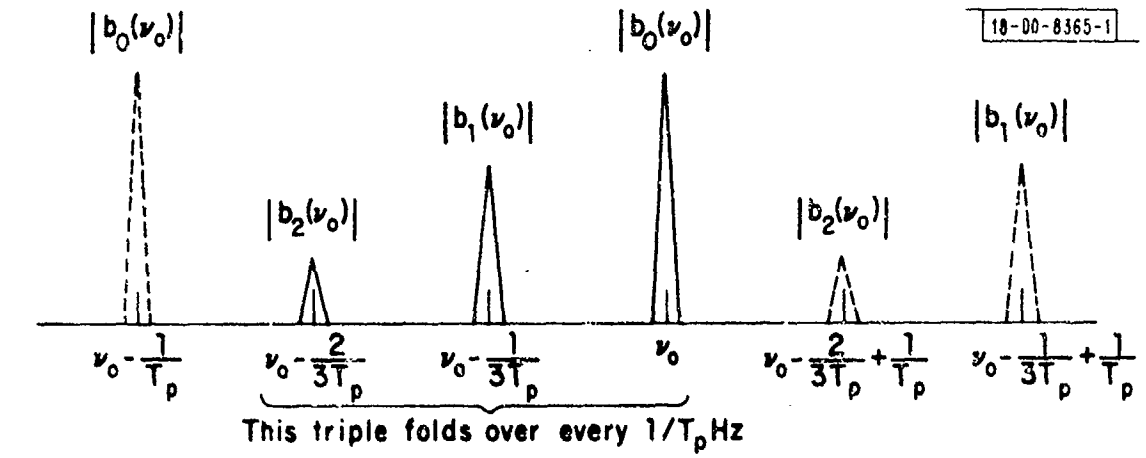

(a)

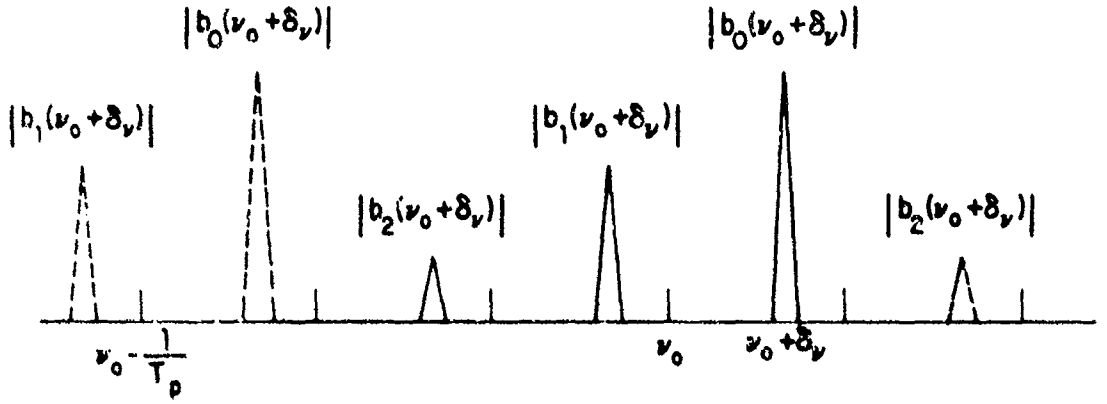

(b)

Fig. 7. (a) Typical target spectrum for three-pulse stagger; (b) Shifted target spectrum for three-pulse stagger.

$$\xi(\tau,\tau_o,\nu_o,\nu_o) = \frac{|\gamma_o|}{T_p^2}\left[\left|b_o(\nu_o)\right|^2 \int_{\nu_o-1/T_p}^{\nu_o} a_o^*(\tau)a_o(\tau_o)\left|F_g(f-\nu_o)\right|^2 e^{j2\pi f(\tau-\tau_o)}df\right.$$

$$+ \left|b_1(\nu_o)\right|^2 \int_{\nu_o-1/T_p}^{\nu_o} a_1^*(\tau)a_1(\tau_o)\left|F_g(f-\nu_o+\frac{1}{3T_p})\right|^2 e^{j2\pi f(\tau-\tau_o)}df$$

$$\left.+ \left|b_2(\nu_o)\right|^2 \int_{\nu_o-1/T_p}^{\nu_o} a_2^*(\tau)a_2(\tau_o)\left|F_g(f-\nu_o+\frac{2}{3T_p})\right|^2 e^{j2\pi f(\tau-\tau_o)}df\right] \tag{60}$$

Assuming the τ takes on only integral values of T_p, then from (18a)

$$a_k(\tau) = e^{-j2\pi\frac{kI(\tau)}{M}} = e^{-j2\pi\frac{k\tau}{MT_p}} \tag{61}$$

It then follows that

$$\int_{\nu_o-1/T_p}^{\nu_o} a_k^*(\tau)a_k(\tau_o)\left|F_g(f-\nu_o+\frac{k}{MT_p})\right|^2 e^{j2\pi f(\tau-\tau_o)}df$$

$$= e^{j2\pi\nu_o(\tau-\tau_o)} R_g(\tau-\tau_o) \tag{62}$$

where

$$R_g(\tau) = \int_{-1/2T_p}^{1/2T_p} \left|F_g(f)\right|^2 e^{j2\pi f\tau} df \tag{63}$$

In Part I it was shown that this function was precisely the autocorrelation function of the two-way antenna pattern. Then the ambiguity function when the signals are matched in Doppler is

$$\left|\xi(\tau,\tau_o,\nu_o,\nu_o)\right| = \frac{\left|\gamma_o\right|}{T_p} R_g(\tau-\tau_o) \left[\left|b_o(\nu_o)\right|^2 + \left|b_1(\nu_o)\right|^2 + \left|b_2(\nu_o)\right|^2\right] \tag{64}$$

where from (18b)

$$b_k(\nu) = \frac{1}{M} \sum_{m=o}^{M-1} e^{-j2\pi\frac{km}{M}} e^{-j2\pi\nu\varepsilon_m} \tag{65}$$

It is shown in the Appendix that

$$\sum_{k=o}^{M-1} \left|b_k(\nu)\right|^2 = 1 \tag{66}$$

hence

$$\left|\xi(\tau,\tau_o,\nu_o,\nu_o)\right| = \frac{\left|\gamma_o\right|}{T_p^2} R_g(\tau-\tau_o) \tag{67}$$

a result which is intuitively satisfying.

In order to evaluate the ambiguity function at other values of ν, it is useful to think of gradually increasing ν from its value at ν_o. For example, when $\nu_o < \nu < 1/3\ T_p$, the absolute value of $Z_s(f;\tau,\nu)$ is shown in Figure 7b. When the correlation operation is performed to evaluate (59) for these values, there will be no spectral overlap and the ambiguity function will essentially be zero. No significant contribution will be made to the ambiguity function until $\nu = \nu_o + 1/3T_p$. In this case, different frequency coefficients line up and (59) becomes

$$\xi(\tau,\tau_o,\nu_o + \tfrac{1}{3T_p},\nu_o) = \frac{\gamma_o}{T_p}\left[b_1^*(\nu_o + \tfrac{1}{3T_p})b_o(\nu_o)\int_{\nu_o-1/T_p}^{\nu_o} a_1^*(\tau)a_o(\tau_o)\left|F_g(f-\nu_o)\right|^2 e^{j2\pi f(\tau-\tau_o)}df\right.$$

$$+ b_2^*(\nu_o + \tfrac{1}{3T_p})b_1(\nu_o)\int_{\nu_o-1/T_p}^{\nu_o} a_2^*(\tau)a_1(\tau_o)\left|F_g(f-\nu_o+\tfrac{1}{3T_p})\right|^2 e^{j2\pi f(\tau-\tau_o)}df$$

$$\left.+ b_o^*(\nu_o + \tfrac{1}{3T_p})b_2(\nu_o)\int_{\nu_o-1/T_p}^{\nu_o} a_o^*(\tau)a_2(\tau_o)\left|F_g(f-\nu_o+\tfrac{2}{3T_p})\right|^2 e^{j2\pi f(\tau-\tau)}df\right] \qquad (68)$$

From (61) it follows that

$$a_{k+1}^{*}(\tau)a_k(\tau_o) = e^{j2\pi\frac{k(\tau-\tau_o)}{MT_p}} e^{j2\pi\frac{\tau}{MT_p}} \tag{69}$$

and therefore

$$\int_{\nu_o-1/T_p}^{\nu_o} a_{k+1}^{*}(\tau)a_k(\tau_o)\left|F_g(f-\nu_o+\frac{k}{MT_p})\right|^2 e^{j2\pi f(\tau-\tau_o)}df$$

$$= e^{j2\pi\nu_o(\tau-\tau_o)} e^{j2\pi\frac{\tau}{MT_p}} R_g(\tau-\tau_o) \tag{70}$$

The ambiguity function is then

$$\left|\xi(\tau,\tau_o,\nu_o+\frac{1}{3T_p},\nu_o)\right| = \frac{|\gamma_o|}{T_p^2} R_g(\tau-\tau_o)\left[\left|b_1^{*}(\nu_o+\frac{1}{3T_p})b_0(\nu_o)\right.\right.$$

$$+ b_2^{*}(\nu_o+\frac{1}{3T_p})b_1(\nu_o)$$

$$\left.\left.+ b_0^{*}(\nu_o+\frac{1}{3T_p})b_2(\nu_o)\right|\right] \tag{71}$$

The next step is to set $\nu = \nu_o + \frac{2}{3T_p}$ and repeat the above operations. In this case, the coefficients are displaced by two and the ambiguity function becomes

$$\left|\xi(\tau,\tau_o,\nu_o + \frac{2}{3T_p},\nu_o)\right| = \frac{|\gamma_o|}{T_p^2} R_g(\tau-\tau_o)\left[\left|b_2^*(\nu_o + \frac{2}{3T_p})b_o(\nu_o)\right.\right.$$

$$+ b_o^*(\nu_o + \frac{2}{3T_p})b_1(\nu_o)$$

$$\left.\left. + b_1^*(\nu_o + \frac{2}{3T_p})b_2(\nu_o)\right|\right] \qquad (72)$$

This process continues ad infinitum and it is possible to deduce a rule for generating the ambiguity function. In the M-pulse stagger case, it becomes

$$\left|\xi(\tau,\tau_o,\nu_o + \frac{m+nM}{MT_p},\nu_o)\right| = \frac{|\gamma_o|}{T_p^2} R_g(\tau-\tau_o)\left|\sum_{k=o}^{M-1} b_{k+m}^*(\nu_o + \frac{m+nM}{MT_p})b_k(\nu_o)\right| \qquad (73)$$

where for positive values of $n = 0,1,2,\cdots$, m takes on the values $m = 0,1,2,\cdots,M-1$, and for negative values of $n = -1,-2,\ldots$, $m = M-1, M-2, 0$. In (73) use has been made of the fact that

$$b_{k+m}(\nu) = b_{(k+m) \text{ modulo } M}(\nu) \qquad (74)$$

which follows directly from (65). It is shown in the Appendix that (73) can be reduced to

$$\left|\xi(\tau,\tau_o,\nu_o+\frac{m+nM}{MT_p},\nu_o)\right| = \frac{|\nu_o|}{T_p^2}R_g(\tau-\tau_o)\cdot\frac{1}{M}\left|\sum_{k=o}^{M-1} e^{j2\pi\frac{m+nM}{MT_p}(kT_p+\varepsilon_k)}\right| \qquad (75)$$

which is a function only of the differences, $\tau-\tau_o$ and $\nu-\nu_o$, and the stagger parameters ε_o, ε_1, $\cdots$, ε_{M-1}. It can be deduced immediately that the ambiguity function is unchanged if $\varepsilon_o = o$, hence for an M-pulse stagger there are M-1 parameters that can be chosen to shape the ambiguity surface.

For the special case of a two-pulse stagger (75) reduces to

$$\left|\xi(\tau-\tau_o,\nu-\nu_o)\right| = \frac{|\nu_o|}{T_p^2}R_g(\tau-\tau_o)\begin{cases}\left|\cos\frac{\pi n\epsilon}{T_p}\right| & \text{if } \nu = \nu_o+\frac{n}{T_p}\\ \left|\sin\pi\frac{2n+1}{2T_p}\epsilon\right| & \text{if } \nu = \nu_o+\frac{n}{T_p}-\frac{1}{2T_p}\end{cases} \qquad (76)$$

and this is sketched in Figure 8a and compared with the ambiguity function for the uniformly sampled case in which $\epsilon = o$, in Figure 8b. It is clear therefore that Doppler resolution is theoretically possible. Whether or not the stagger parameters can be chosen to force the subsidiary side-lobes below a practically useful level is, however, a separate question. It is of interest to examine the ambiguity function of higher order stagger sequences that are currently used in practice. The results for the ASR-7 radar, that uses a 6-pulse stagger are shown in Figure 9.

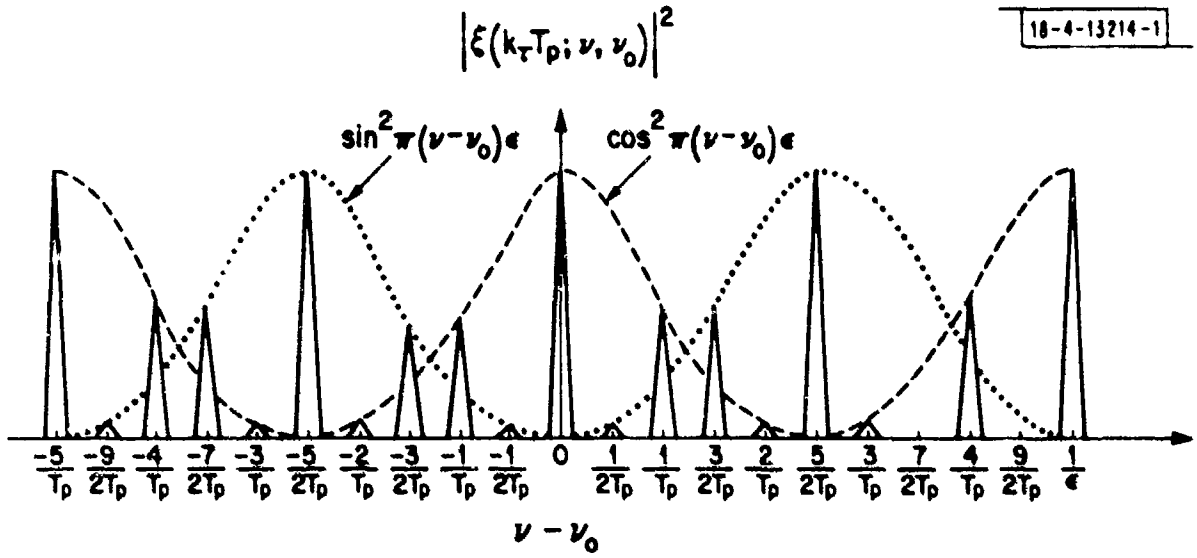

(a) Two-pulse staggered PRF.

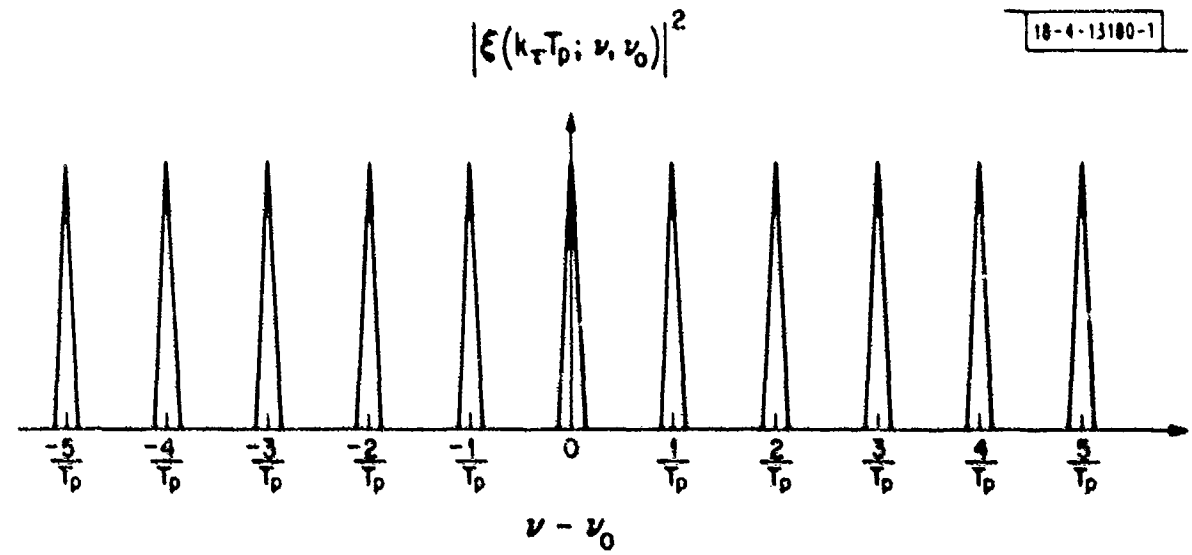

(b) Uniform PRF.

Fig. 8. MTI ambiguity function.

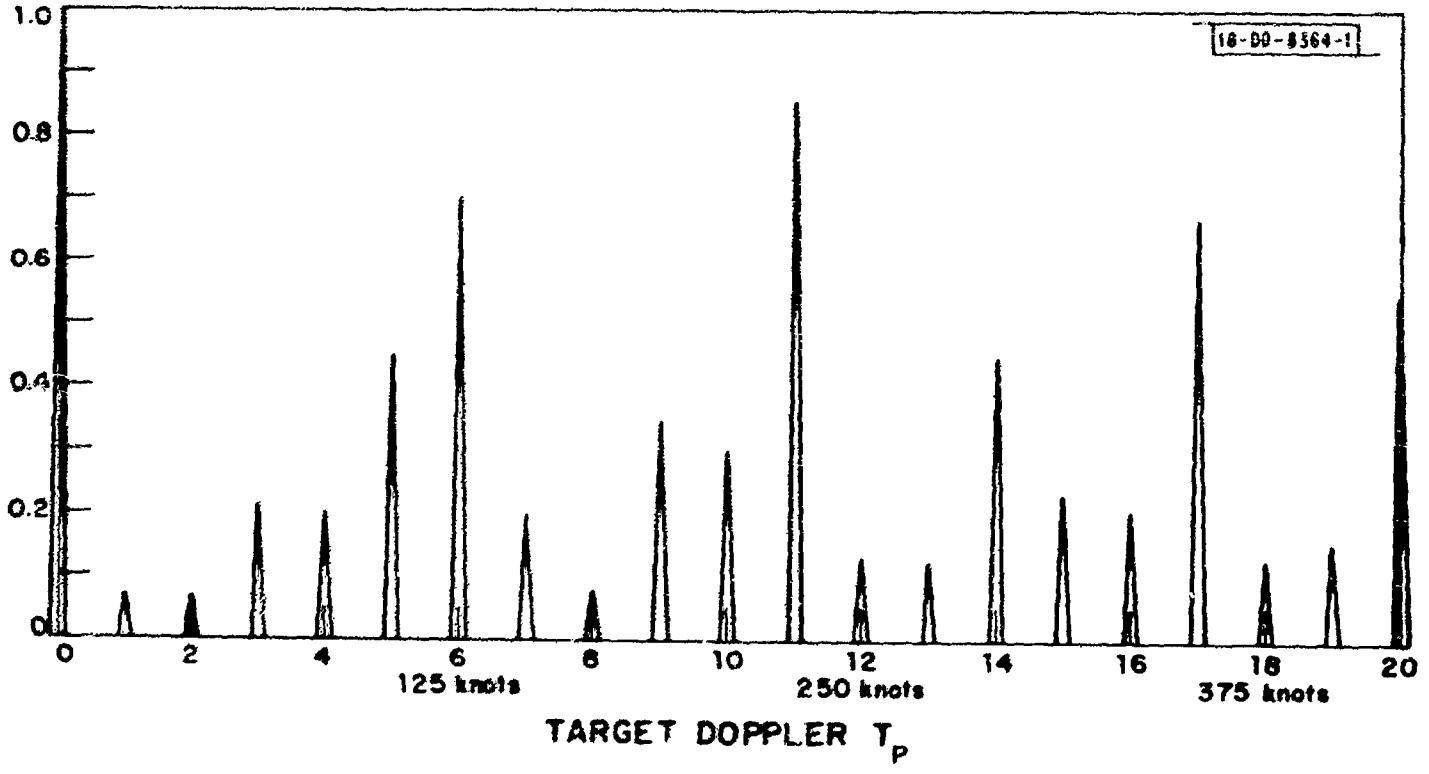

Fig. 9. Ambiguity function for the ASR-7 using an operational six-pulse stagger.

The Matched Filter-Clutter Filter Ambiguity Function

In the preceding section, the ambiguity function for the clutter-free case was derived. This is a useful characterization when the signal is designed to function in only a white-noise environment as it is then clear that all of the side-lobes should be made uniformly low. The more typical situation for MTI requires a characterization that includes the clutter in the analysis. If the ambiguity function is viewed as the delay-Doppler energy distribution of the signal out of the optimum processor, then it is clear that the effect of the clutter is to add notch filters at multiples of the PRF's. Then the more general ambiguity function is given by

$$\xi(\underline{\alpha},\underline{\alpha}_0) = \int_{-1/2T_p}^{1/2T_p} H_c(f) Z_s^*(f;\underline{\alpha}) Z_s(f;\underline{\alpha}_0) df \tag{77}$$

As in the clutter-free problem the general result will be obtained by extending the arguments made for the three-pulse staggered case. This is most easily done by writing a general expression for (60) and (68) from which the ambiguity function is deduced. This expression is

$$\xi(\tau,\tau_0,\nu_0 + \frac{m+nM}{MT_p},\nu_0) =$$

$$\frac{\gamma_0}{T_p} \sum_{k=0}^{M-1} b_{k+m}^*(\nu_0 + \frac{m+nM}{MT_p}) b_k(\nu_0) \int_{\nu_0 - 1/T_p}^{\nu_0} a_{k+m}^*(\tau) a_k(\tau_0) \left| F_g(f - \nu_0 + \frac{k}{MT_p}) \right|^2 H_c(f) e^{j2\pi f(\tau-\tau_0)} df \tag{78}$$

For the purpose of this discussion it is reasonable to assume that the clutter filter transfer function changes slowly over the width of the signal spectrum, hence allowing the following approximation for the last term in (78)

$$H_c(\nu_o - \frac{k}{MT_p}) \int_{\nu_o - 1/T_p}^{\nu_o} a^*_{k+m}(\tau) a_k(\tau_o) \left| F_g(f - \nu_o + \frac{k}{MT_p}) \right|^2 e^{j2\pi f(\tau - \tau_o)} df$$

$$= H_c(\nu_o - \frac{k}{MT_p}) e^{j2\pi\nu_o(\tau-\tau_o)} e^{j2\pi\frac{m\tau}{MT_p}} R_g(\tau - \tau_o) \qquad (79)$$

where the last equation follows from a generalization of (60) and (68). Then the ambiguity function is

$$\left| \xi(\tau, \tau_o, \nu_o + \frac{m+nM}{MT_p}, \nu_o) \right| =$$

$$\frac{\gamma_o}{T_p^2} R_g(\tau - \tau_o) \left| \sum_{k=0}^{N-1} b^*_{k+m}(\nu_o + \frac{m+nM}{MT_p}) b_k(\nu_o) H_c(\nu_o - \frac{k}{MT_p}) \right| \qquad (80)$$

To evaluate (80) it is assumed that the clutter filter is well modelled by a notch at DC as well as at all multiples of the PRF. The approximation was developed in conjunction with the evaluation of the SIR for staggered PRF's.

Suppose now that

$$\nu_o - \frac{k}{MT_p} \neq \frac{n}{T_p} \qquad k = 0,1,\cdots,M-1 \tag{81}$$

holds for every n, then

$$H_c(\nu_o - \frac{k}{MT_p}) \cong 1 \tag{82}$$

and (80) reduces to the clutter-free ambiguity function. If for some value of k, k' say,

$$\nu_o - \frac{k'}{MT_p} = \frac{n}{T_p} \tag{83}$$

for some value of n, then

$$H_c(\nu_o - \frac{k'}{MT_p}) \approx 0 \tag{84}$$

and (80) reduces to

$$\left|\xi(\tau,\tau_o,\nu_o + \frac{m+nM}{MT_p},\nu_o)\right| = \frac{\gamma_o}{T_p} R_g(\tau-\tau_o)\left|\sum_{\substack{k=0 \\ k\neq k'}}^{M-1} b^*_{k+m}(\nu_o + \frac{m+nM}{MT_p}) b_k(\nu_o)\right| \tag{85}$$

This function is much more difficult to plot as it depends on the true target Doppler rather than just the difference between the true and tested values.

In fact, for an M-pulse stagger, (M+1) cuts of the ambiguity function are needed to describe it completely.

MTI Signal Design

In the clutter-free case, it is clear that the stagger parameters should be chosen to produce an ambiguity surface with uniformly low Doppler side-lobes. From (73) this reduces to the problem of picking the stagger parameters $\varepsilon_0, \varepsilon_1, \cdots, \varepsilon_{M-1}$ so that

$$\left| \frac{1}{M} \sum_{k=0}^{M-1} e^{j2\pi \frac{m+nM}{MT_p}(kT_p + \varepsilon_k)} \right| \leq \delta \tag{86}$$

where for 20dB sidelobes δ would be -1, etc. This signal design problem has much in common with design of antenna patterns using an array with non-uniformly spaced elements. This is a difficult problem to solve and it is expected that when the clutter filter is added, it would be even more difficult to simultaneously design the (M+1) folds of the cluttered ambiguity function. A simpler design strategy can be obtained from the SIR analysis in Section III where it was shown that the degradation in the performance was given by (50). From this expression it is clear that the stagger parameters could be chosen to minimize the depths of the notches by minimizing the functions

$$\left| b_m\left(\frac{m+nM}{MT_p}\right) \right| = \left| \frac{1}{M} \sum_{k=0}^{M-1} e^{-j2\pi \frac{mk}{M}} \; e^{-j2\pi \frac{m+nM}{MT_p} \epsilon_k} \right| \tag{87}$$

which follows from the definition of $b_m(\nu)$ in (65). This expression can easily be manipulated to take exactly the same form as that in (86). This is interesting as it shows that the simple criterion of uniformly low sidelobes is a good signal design strategy in the cluttered as well as the white noise environments.

Unfortunately, time did not permit the thorough examination of these signal design problems. Therefore, as of this writing, their solution remains an unanswered question and it will be necessary to be content to use the NTI ambiguity function as a tool for signal analysis, and only indirectly for signal synthesis.

APPENDIX

In order to evaluate the MTI ambiguity function it was claimed in (75) that

$$\sum_{k=o}^{M-1} b_{k+m}^{*}\left(\nu_o + \frac{m+nM}{MT_p}\right) b_k(\nu_o) \triangleq \psi\left(\nu_o + \frac{m+nM}{MT_p},\ \nu_o\right)$$

$$= \frac{1}{M}\sum_{k=o}^{M-1} e^{j2\pi\frac{m+nM}{MT_p}(kT_p+\varepsilon_m)} \qquad m = 0,1,\cdots,M-1 \qquad \text{(A-1)}$$

where from (65)

$$b_k(\nu) = \frac{1}{M}\sum_{p=o}^{M-1} e^{-j2\pi\frac{kp}{M}} e^{-j2\pi\nu\varepsilon_p} \qquad \text{(A-2)}$$

It is the purpose of this section to prove (A-1) and hence deduce that

$$\sum_{k=o}^{M-1} \left|b_k(\nu)\right|^2 = 1 \qquad \text{(A-3)}$$

as stated in (48 and (66). To begin, vectors and matrices are defined as follows:

$$\underline{g}(\nu) = \left(e^{-j2\pi\nu\varepsilon_o},\ e^{-j2\pi\nu\varepsilon_1},\ \cdots,\ e^{-j2\pi\nu\varepsilon_{M-1}}\right)' \qquad \text{(A-4)}$$

$$\underline{x}^m(\nu) = \left[b_m(\nu),\ b_{m+1}(\nu),\ \cdots,\ b_{m+M-1}(\nu)\right]' \qquad \text{(A-5)}$$

$$(M^m)_{kp} = \frac{1}{M} e^{-j2\pi(k+m)\frac{p}{M}} \tag{A-6}$$

where m, k and p take on values $0,1,2,\cdots,M-1$. First, from (A-2) it is noted that

$$b_{k+m}(\nu) \triangleq \frac{1}{M}\sum_{p=0}^{M-1} e^{-j2\pi\frac{(k+m)p}{M}} e^{-j2\pi\nu\epsilon_p}$$

$$= \sum_{p=0}^{M-1} M^m_{kp}\beta_p(\nu)$$

$$= \chi_k{}^m(\nu) \tag{A-7}$$

where use has been made of the fact that

$$b_{k+m}(\nu) = b_{(k+m)\ \text{modulo } M}(\nu) \tag{A-8}$$

Hence

$$\chi^{(m)}(\nu) = M^m\underline{\beta}(\nu) \tag{A-9}$$

If $\langle \underline{u}, \underline{v} \rangle$ denotes the inner product in C^M, then

$$\psi(\nu_o + \frac{m+nM}{MT_p}, \nu_o) = \langle \underline{\chi}^m(\nu_o + \frac{m+nM}{MT_p}), \underline{\chi}^o(\nu_o)$$

$$= \langle M^m \underline{\beta}(\nu_o + \frac{m+nM}{MT_p}), M^o \underline{\beta}(\nu_o)$$

$$= \langle M^{o^*} M^m \underline{\beta}(\nu_o + \frac{m+nM}{MT_p}), \underline{\beta}(\nu_o) \rangle \qquad \text{(A-10)}$$

where * denotes conjugate transpose. Now let

$$Q^m = M^{o^*} M^m \qquad \text{(A-11)}$$

Then

$$Q^m_{kl} = \sum_{p=o}^{M-1} \left(M^{o^*}\right)_{kp} \left(M^m\right)_{p\ell}$$

$$= \sum_{p=o}^{M-1} \left(M^o\right)^*_{pk} \left(M^m\right)_{p\ell}$$

$$= \sum_{p=o}^{M-\ell} \frac{1}{M} e^{j2\pi \frac{pk}{M}} \frac{1}{M} e^{-j2\pi \frac{(p+m)\ell}{M}}$$

$$= \left[\frac{1}{M} e^{-j2\pi\frac{m\ell}{M}}\right]\left[\frac{1}{M}\sum_{p=0}^{M-1} e^{j2\pi\frac{(k-\ell)p}{M}}\right] \tag{A-12}$$

If $k = \ell$, then

$$Q_{kk}^{m} = \frac{1}{M} e^{-j2\pi\frac{mk}{M}} \tag{A-13}$$

For the case when $k \neq \ell$, the second term in (A-12) can be evaluated by setting

$$v = e^{j\frac{2\pi}{M}(k-\ell)} \tag{A-14}$$

and noting that

$$\sum_{p=0}^{M-1} e^{j2\pi\frac{(k-\ell)p}{M}} = \sum_{p=0}^{M-1} v^{p} = \frac{1-v^{M}}{1-v} = 0 \tag{A-15}$$

Hence $Q_{k\ell}^{m} = 0$ when $k \neq \ell$ and therefore the matrix Q^{m} is diagonal for all m.
Using this result in (A-10) yields

$$\psi(\nu_o + \frac{m+nM}{MT_p}, \nu_o) = \sum_{k=0}^{M-1}\left[Q_{kk}^{m}\beta_k(\nu_o + \frac{m+nM}{MT_p})\right]^{*}\beta_k(\nu_o)$$

$$= \frac{1}{M}\sum_{k=0}^{M-1} e^{j2\pi\frac{mk}{M}}\beta_k^{*}(\nu_o + \frac{m+nM}{MT_p})\beta_k(\nu_o)$$

$$= \frac{1}{M}\sum_{k=0}^{M-1} e^{j2\pi\frac{mk}{M}} e^{j2\pi\frac{m+nM}{MT_p}\varepsilon_k}$$

$$= \frac{1}{M}\sum_{k=0}^{M-1} e^{j2\pi\frac{m+nM}{MT_p}(kT_p + \varepsilon_k)} \qquad \text{(A-16)}$$

as required.

ACKNOWLEDGMENTS

The author would like to thank R.D. Yates whose critical review of the draft of Part II resulted in a significant improvement in the published version. It is noted with appreciation that a suggestion by J.R. Johnson led to the spectrum of the staggered PRF transmitted signal. Finally, the author would like to thank T.J. Goblick for the many interesting and useful conversations that took place during the course of this work.

REFERENCES

[1] R. J. McAulay, "A Theory for Optimal MTI Digital Signal Processing, Part I: Receiver Synthesis," Technical Note 1972-14, Lincoln Laboratory, M.I.T. (22 February 1972).

[2] M.I. Skolnik, Introduction to Radar Systems, (McGraw Hill Book Co., New York, 1962), Chapter 4.

[3] S.E. Perlman, "Staggered Rep Rate Fills Radar Blind Spots," Electronics, 21 November 1958, pp. 82-85.

[4] Air Route Surveillance Radar ARSR-2, Vol. I, General Description and Theory of Operation, Raytheon Company, 1960.

DOCUMENT CONTROL DATA - R&D

(Security classification of title, body of abstract and indexing annotation must be entered when the overall report is classified)

1. ORIGINATING ACTIVITY *(Corporate author)* Lincoln Laboratory, M.I.T.	2a. REPORT SECURITY CLASSIFICATION Unclassified 2b. GROUP None

3. REPORT TITLE

A Theory for Optimal MTI Digital Signal Processing.
Part II: Signal Design

4. DESCRIPTIVE NOTES *(Type of report and inclusive dates)*

Technical Note

5. AUTHOR(S) *(Last name, first name, initial)*

McAulay, Robert J.

6. REPORT DATE	7a. TOTAL NO. OF PAGES	7b. NO. OF REFS
4 October 1972	58	4

8a. CONTRACT OR GRANT NO. F19628-73-C-0002 b. PROJECT NO. 649L c. d.	9a. ORIGINATOR'S REPORT NUMBER(S) Technical Note 1972-14 (Part II) 9b. OTHER REPORT NO(S) *(Any other numbers that may be assigned this report)* ESD-TR-72-217

10. AVAILABILITY/LIMITATION NOTICES

Approved for public release; distribution unlimited.

11. SUPPLEMENTARY NOTES	12. SPONSORING MILITARY ACTIVITY
Supplement to ESD-TR-72-55	Air Force Systems Command, USAF

13. ABSTRACT

In Part I of this report the optimum MTI receiver was derived and analyzed for the case in which the radar pulses were emitted from the transmitter equally spaced in time. For typical long range ATC surveillance radars, aliasing of the target and clutter spectra results in detection blind speeds at multiples of approximately 70 knots. It is well known operationally that these blind speeds can be eliminated by staggering the transmitter PRF. Heretofore, there has been no thorough theoretical analysis of the effect of staggered PRF on the spectral distribution of the target and clutter signals. It is shown in Part II that the clutter spectral density continues to fold over at the PRF, but that the signal spectrum becomes dispersed in frequency, somewhat like an anti-jam signal. The effect that this phenomenon has on the performance of the optimum processor is evaluated in terms of the signal-to-interference ratio (SIR) criterion that was derived in Part I.

It is further noted that even when the target Doppler shifts are more than one PRF apart, the spectra are distinguishable, suggesting that unambiguous Doppler estimation may be possible. This concept is explored in detail using the MTI ambiguity function. It is shown that good SIR performance can be obtained by choosing the stagger parameters to minimize the height of the subsidiary Doppler side-lobes. The resulting design problem is noted to be similar to that of obtaining good antenna patterns for arrays having non-uniformly spaced elements.

14. KEY WORDS

digital signal processing
air traffic control
MTI (moving target indicator)
PRF (pulse repetition frequency)
SIR (signal to interference ratio)

UNCLASSIFIED